Proton NMR and Dynamic Studies of Hydrous Ruthenium Oxide

Riqiang Fu,*,† Zhiru Ma,† and Jim P. Zheng‡

Center for Interdisciplinary Magnetic Resonance, National High Magnetic Field Laboratory, 1800 East Paul Dirac Drive, Tallahassee, Florida 32310, and Department of Electrical and Computer Engineering, Florida A&M University and Florida State University, Tallahassee, Florida 32310

Received: October 17, 2001; In Final Form: January 31, 2002

A series of hydrous ruthenium oxide ($RuO_2 \cdot xH_2O$) samples annealed at different temperatures have been studied by solid-state ^1H NMR spectroscopy. The proton dynamics of the $RuO_2 \cdot xH_2O$ samples was characterized for the first time through variable-temperature ^1H spin−lattice relaxation time (T_1) measurements. For the $RuO_2 \cdot xH_2O$ samples annealed at temperatures lower than 100 °C and higher than 200 °C, a high proton activation energy was obtained, implying that the proton dynamics/diffusive motion is relatively restrained, whereas the samples annealed at temperatures between 100 and 200 °C exhibited relatively low proton activation energies, indicating that the protons can easily diffuse into the bulk of the material. Therefore, the proton activation energy correlates strongly with the hydrogen transfer and storage ability of the proton-conducting materials. In combination with electrochemical measurements, our NMR data also suggest that the coexistence of the Ru^{2+}, Ru^{3+}, and Ru^{4+} valency states in the local structure of the $RuO_2 \cdot xH_2O$ is crucial for hydrogen transfer and storage ability.

Introduction

Recently, there has been increasing interest in electrochemical (EC) supercapacitors because of their long cycle life and high power density.[1] EC capacitors have important technological applications, such as electric and hybrid vehicles, digital communication devices, and backup power sources.[1−3] Of the electrode materials used in EC capacitors, hydrous ruthenium oxide ($RuO_2 \cdot xH_2O$) is one of the best because of its high specific capacitance, high conductivity, good electrochemical reversibility, and high power and energy density.[4−8] A maximum specific capacitance of 768 F/g was obtained from an amorphous $RuO_2 \cdot xH_2O$ sample, which was more than twice as large as the values obtained from other capacitive electrode materials.[4] On the basis of electrochemical analyses,[4−8] it was believed that the high specific capacitance of $RuO_2 \cdot xH_2O$ results from the diffusion and intercalation of protons into the bulk of the material. In contrast, the proton reactions are limited to the surface of the anhydrous ruthenium oxide material. However, this is still a largely qualitative theory to explain why hydrous ruthenium oxide is superior to the crystalline material. It was also found that the specific capacitance of $RuO_2 \cdot xH_2O$ is also strongly affected by the hydrogen concentration[5,9] and by doping[4,10] as well.

Despite its important technological applications in charge storage and electrocatalysis,[11,12] there have been only a few publications in the literature so far for understanding $RuO_2 \cdot xH_2O$ materials. These materials have not been well characterized largely because of their amorphous nature and composition variability. Mckeown et al.[13] characterized the structures of the hydrous ruthenium oxides $RuO_2 \cdot 2.32H_2O$ and $RuO_2 \cdot 0.29H_2O$ and anhydrous RuO_2 by the combined use of thermogravimetric analysis (TGA), X-ray diffraction (XRD), X-ray absorption near-edge structure (XANES), and extended X-ray fine structure (EXAFS) analyses. It was found that the local structures of $RuO_2 \cdot 2.32H_2O$ and $RuO_2 \cdot 0.29H_2O$ are remarkably different because of the presence of the structural water. However, because the orientation of the water molecules can not be discerned from the EXAFS data, the relation between the structural water and the proton charge storage of $RuO_2 \cdot xH_2O$ is still not clear. In addition, ^2D NMR spectra of a series of isotope-exchanged $RuO_2 \cdot xD_2O$ and $D_\delta RuO_2 \cdot xD_2O$ samples indicated substantial molecular mobility in the materials.[14] In our previous work,[9] we observed the $^1H/^2D$ line widths of solid-state static $^1H/^2D$ NMR spectra of $RuO_2 \cdot xH_2O$ under various experimental conditions. By correlating the $^1H/^2D$ line widths with the specific capacitance measurements at different temperatures, we concluded that the mobility of the water molecules and their interaction with the ruthenium oxides play an important role in the proton charge density.

Nuclear magnetic resonance (NMR) spectroscopy[15−20] has become a well-established technique for characterizating the dynamics and obtaining detailed structural information on materials even in an amorphous phase. In the present work, we measured the proton spin−lattice relaxation times (T_1) of the $RuO_2 \cdot xH_2O$ materials at different temperatures and then characterized the proton dynamics of the $RuO_2 \cdot xH_2O$ materials through relaxation analysis. The results were further interpreted in combination with electrochemical measurements for a better understanding of the structural details of the materials, as well as the relationship between the proton dynamics and the proton charge storage.

Materials and Experiments

A sample of $RuO_2 \cdot 2.76H_2O$ (Ru 55.29%) was purchased from Alfa Aesar/Johnson Matthey Company and was used without further purification. A series of hydrous ruthenium oxide $RuO_2 \cdot xH_2O$ samples with different compositions x were prepared by an annealing process. Only the water in the sample is lost during

* Corresponding author. E-mail: rfu@magnet.fsu.edu. Fax: (850)644-1366.
† National High Magnetic Field Laboratory.
‡ Florida A&M University and Florida State University.

10.1021/jp013860q CCC: $22.00
Published on Web 03/08/2002

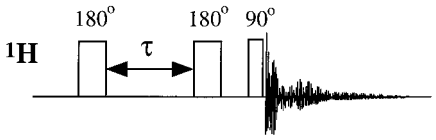

Figure 1. Pulse sequence used for inversion recovery T_1 measurements. A second 180° pulse was applied after the recovery time τ followed by a short delay of 10 μs to suppress the ^{1}H background signals from outside the sample coil, as explained in the text.

the annealing process, so that the water content x can be calculated from the weight change of the sample upon annealing. The original $RuO_2 \cdot 2.76H_2O$ sample was weighed and heated in an oven at different temperatures for about 24 h. Eleven $RuO_2 \cdot xH_2O$ samples annealed at different temperatures ranging from 25 to 300 °C were used in the experiments.

Cyclic voltammetry (CV) experiments were used to measure the specific capacitance of $RuO_2 \cdot xH_2O$[4,9] by using a three-electrode system with a saturated calomel electrode (SCE), a platinum plate, and the $RuO_2 \cdot xH_2O$ as the reference, counter, and working electrodes, respectively. The working electrode was made from $RuO_2 \cdot xH_2O$ powder mixed with about 5% Teflon binder and then pressed on Pt mesh. The electrolyte used in the measurement was 0.5 M H_2SO_4 solution. During the CV measurements, the potential between the working and reference electrodes was swept linearly between 1 and 0 V (vs SCE) at a constant scan rate of 2 mV/s. At the same time, the current flowing from the working electrode to the counter electrode was measured. The capacitance of the working electrode was calculated by the ratio of the current to the scan rate. The specific capacitance defines the capacitance per unit weight of the electrode material.

The static ^{1}H NMR measurements were performed on a Bruker DMX 300 NMR spectrometer (B_o = 7 T) with a ^{1}H Larmor frequency of 300 MHz using a 4-mm Bruker CPMAS double-resonance NMR probe. The ^{1}H spin−lattice relaxation times were measured between 200 and 340 K using a modified inversion recovery pulse sequence, as shown in Figure 1, where an additional 180° pulse was applied after the recovery time τ followed by a short delay. The 180° pulse inserted here was used to invert the magnetization resulting from the sample, but it has little effect on the ^{1}H background signals resulting from the probe components outside the sample coil. Therefore, after the signals recorded with and without the 180° pulse are subtracted, the unwanted ^{1}H background signals from the probe components can be suppressed and the longitudinal relaxation of the sample signals can be described by

$$M(\tau) = M(\infty) - [M(\infty) - M(0)] \exp(-t/T_1) \qquad (1)$$

where $M(0)$ and $M(\infty)$ represent the initial and equilibrium magnetizations, respectively, and T_1 is the ^{1}H spin−lattice relaxation time. The 90° and 180° pulse widths were calibrated to be 4 and 8 μs, respectively. All temperatures were controlled to within ±0.1 K by a Bruker BVT-2000 unit. A set of 18 spectra with different recovery times τ was used for each T_1 measurement. Between 16 and 48 scans were accumulated for each spectrum with a recycle delay of 2 s, depending on the samples used in the experiments.

Results and Discussion

Figure 2 shows the specific capacitance as a function of the sample annealing temperature. Clearly, the specific capacitance of the $RuO_2 \cdot xH_2O$ material increased as the sample annealing temperature was increased from 50 to 150 °C, and reached its maximum value at about 150 °C. With further increase of the annealing temperature, the specific capacitance decreased. Both the X-ray diffraction measurements and the high-resolution transmission electron microscope (TEM) images (data not shown) illustrate that the $RuO_2 \cdot xH_2O$ was in an amorphous phase at annealing temperatures lower than 150 °C, whereas RuO_2 crystalline particles began to form at 150 °C and increased in size at higher temperatures. Therefore, the obtained maximum specific capacitance occurs at the transition temperature between the amorphous phase of the $RuO_2 \cdot xH_2O$ and the formation of the RuO_2 crystalline phase, which is consistent with previous studies.[4,5,9]

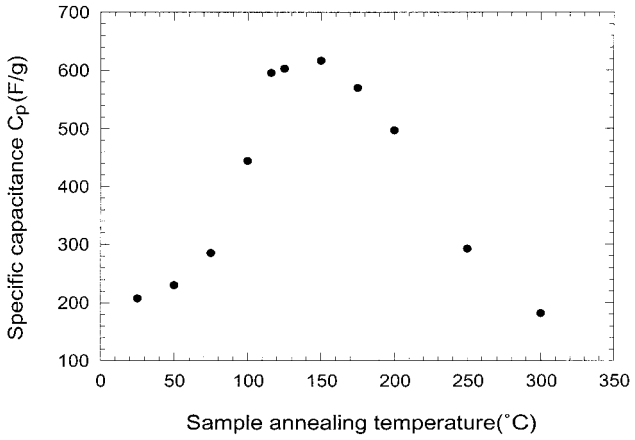

Figure 2. Specific capacitance of the $RuO_2 \cdot xH_2O$ samples as a function of annealing temperature.

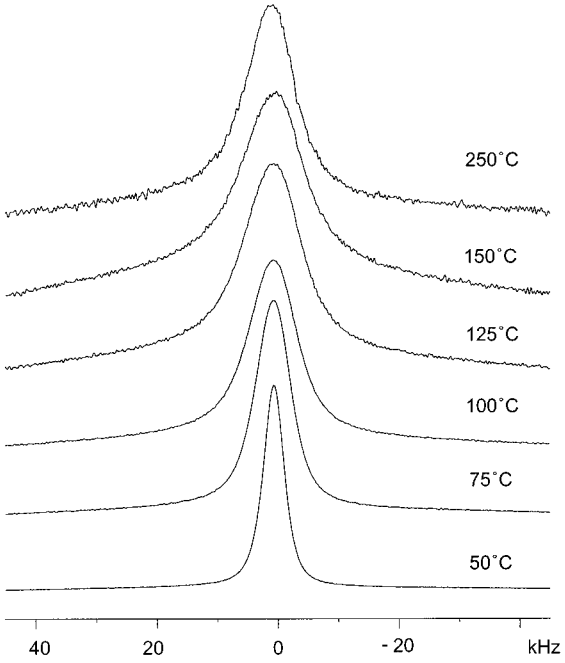

Figure 3. Wide-line ^{1}H NMR spectra of $RuO_2 \cdot xH_2O$ samples annealed at various temperatures. All of the spectra were recorded on a Bruker DMX 300 NMR spectrometer at room temperature (300 K).

Figure 3 shows the static ^{1}H NMR spectra of the $RuO_2 \cdot xH_2O$ samples annealed at different temperatures. Unlike rigid samples, where the typical ^{1}H line width at half-height is several tens of kilohertz,[21] all spectra here exhibit a relatively narrow resonance (<8 kHz line width at half-height). Because these samples are not paramagnetic, the ^{1}H resonance line broadening mainly results from the interproton dipolar interactions. Such a narrow resonance indicates the presence of relatively weak proton−proton dipolar interactions in these materials, thus suggesting

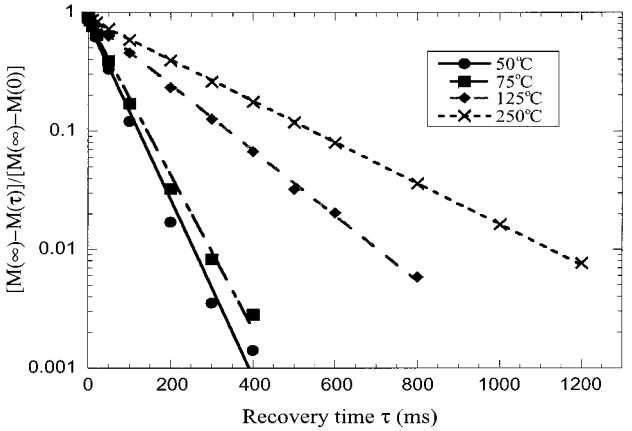

Figure 4. Semilogarithmic plot of normalized integral signal intensities as a function of recovery time. All of the experimental data recorded on a Bruker DMX 300 spectrometer at 300 K were fitted using single exponential component as indicated by the solid lines. The proton spin−lattice relaxation times (T_1) obtained from the measurements were 49.1, 58.7, 146.2, and 238.5 for the $RuO_2{\cdot}xH_2O$ samples annealed at 50, 75, 125, and 250 °C, respectively.

that the hydrogen atoms in the $RuO_2{\cdot}xH_2O$ samples are relatively mobile, compared to those in the rigid samples. The proton−proton dipolar interactions could be further suppressed by the so-called magic angle spinning (MAS)[22] for better resolution. However, it was very difficult to spin the $RuO_2{\cdot}xH_2O$ samples fast enough to suppress the dipolar interactions effectively in a high magnetic field because they are conducting materials.[23] In addition, in systems where electronic states cannot be well defined, every electronic state has a different electronic environment, thus resulting in heterogeneous line broadening. As in Figure 3, the ^{1}H line width gradually increased as the annealing temperature was increased from 50 to 150 °C and reached its maximum at around 150 °C, where the maximum specific capacitance was obtained. With further increase of the annealing temperature, the line width became narrower. This observation suggests that the electronic states of hydrogen depend on the annealing temperature, i.e., the interactions between the water molecules and the RuO_2 lattice are temperature-dependent. Therefore, the ^{1}H line width also illustrates the local structural changes in the electrode materials.

Figure 4 shows the recovery of ^{1}H magnetization from the $RuO_2{\cdot}xH_2O$ samples annealed at 50, 75, 125, and 250 °C recorded on a Bruker DMX 300 spectrometer at 300 K. A single-exponential recovery was found for all measurements, as indicated in Figure 4. Clearly, the ^{1}H signal of the sample annealed at 50 °C recovers much more quickly than that of the sample annealed at 250 °C. The proton spin−lattice relaxation times T_1 obtained were 49.1, 58.7, 146.2, and 238.5 ms for the samples annealed at 50, 75, 125, and 250 °C, respectively. Therefore, the value of ^{1}H T_1 depends strongly on the annealing temperature. With increasing annealing temperature, the ^{1}H T_1 value increases steadily.

To gain insights into the dynamic behavior of the hydrogen in the $RuO_2{\cdot}xH_2O$ electrode materials, the temperature dependence of the static ^{1}H spin−lattice relaxation times of the samples annealed at different temperatures were measured. Figure 5 displays the ^{1}H spin−lattice relaxation time T_1 of the $RuO_2{\cdot}xH_2O$ samples as a function of temperature. It can be noticed in Figure 5 that a T_1 minimum was observed for those samples annealed at lower temperatures (e.g., 50 and 75 °C), but there was not a T_1 minimum within the experimental temperature range for those samples annealed at higher temperatures (e.g., 125 and 250 °C). The T_1 minima appeared at

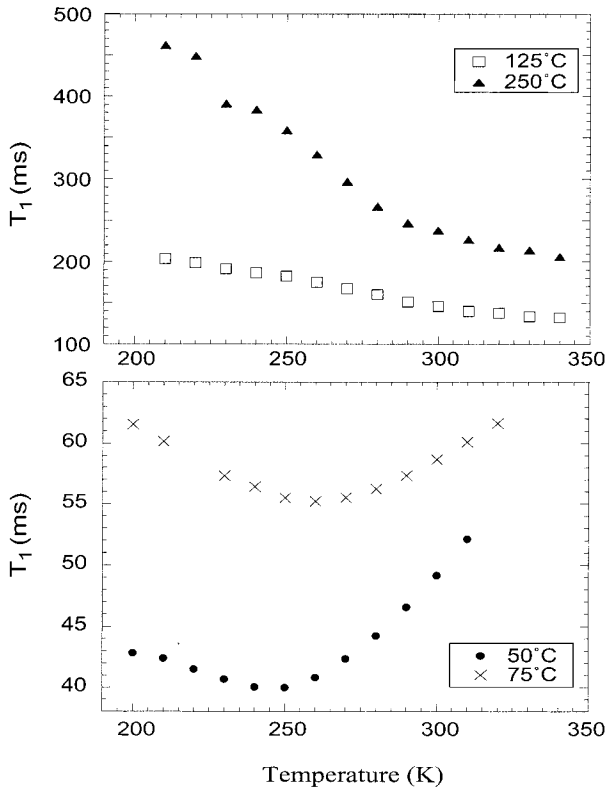

Figure 5. Plots of ^{1}H spin lattice relaxation times (T_1) as a function of temperature. Only the ^{1}H T_1 values obtained from the $RuO_2{\cdot}xH_2O$ samples annealed at 50, 75, 125, and 250 °C are shown in the plots.

about 250 and 260 K for the samples annealed at 50 and 75 °C, respectively. This observation indicates that the molecular motion for these two samples is in the fast-motion regime at 300 K, which is higher than that at the T_1 minimums. On the other hand, for the samples annealed at 125 and 250 °C, the measured T_1 values became smaller as the temperature was increased. Apparently, the T_1 minimum could appear at a temperature higher than 340 K, which implies that, for the samples annealed at temperatures higher than 125 °C, the molecular motion is in the slow-motion regime[24] within this temperature range. It is also interesting to note that the value of the T_1 minimum increased significantly when the sample annealing temperature was increased from 50 to 75 °C. Thus, the proton−proton distance in the $RuO_2{\cdot}xH_2O$ materials becomes longer as the structural water is stripped off at the higher annealing temperature. This observation indicates that the local structure of the $RuO_2{\cdot}xH_2O$ is dependent on the water content.[13]

It is assumed that the interproton dipole−dipole interactions dominate spin−lattice relaxation, which is undoubtedly true for the motions encountered in the $RuO_2{\cdot}xH_2O$ materials. Consequently, the dependence of the relaxation rate $1/T_1$ on the correlation time τ_c can be described by[24−26]

$$\frac{1}{T_1} = C\left(\frac{\tau_c}{1+\omega_0^2\tau_c^2} + \frac{4\tau_c}{1+4\omega_0^2\tau_c^2}\right) \qquad (2)$$

where τ_c is the correlation time describing the dynamic process, ω_0 is the ^{1}H resonance frequency, and C is a dipole−dipole relaxation constant, which is associated with the proton−proton distance according to

$$C = \frac{3}{10}\left(\frac{\mu_0}{4\pi}\frac{\gamma_H^2\hbar}{r_{HH}^3}\right)^2 \qquad (3)$$

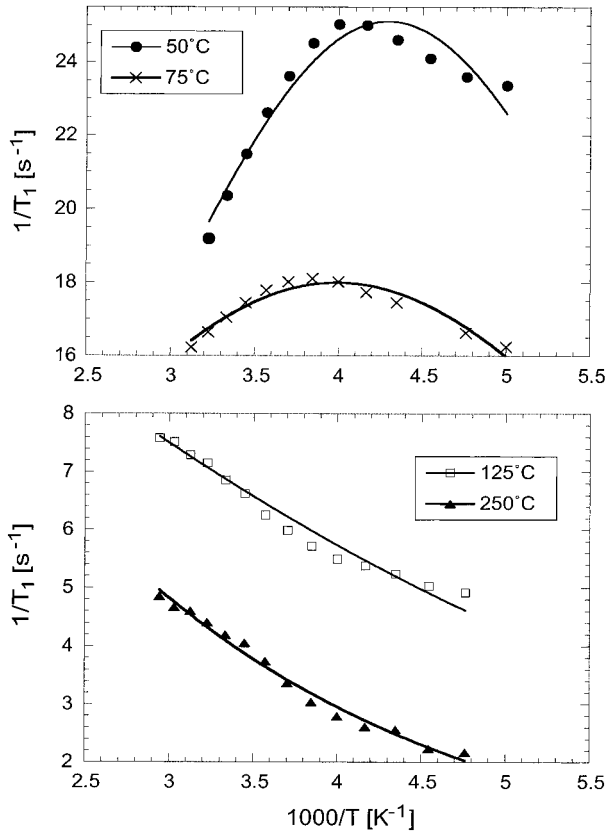

Figure 6. Arrhenius plot of the relaxation rate ($1/T_1$) for the samples annealed at 50, 75, 125, and 250 °C. All of the experimental data were fitted by using eqs 2−4, based on the BBP model.[24] From the fitting indicated by solid lines, the activation energy (E_a) values obtained were 6.11, 4.56, 2.59, and 4.17 kJ/mol, while the proton−proton distances (r_{HH}) were 1.306, 1.389, 1.442, and 1.361 Å for the samples annealed at 50, 75, 125, and 250 °C, respectively.

where γ_H is the proton gyromagnetic ratio and r_{HH} is the proton−proton distance.

For thermally activated diffusion, the correlation time τ_c is usually described in an Arrhenius form

$$\tau_c = \tau_0 \exp(E_a/RT) \tag{4}$$

where τ_0 is the prefactor, R is the gas constant, T is the absolute temperature, and E_a refers to the activation energy (per mole) for the dynamic process.

Figure 6 shows the relaxation rate ($1/T_1$) in the Arrhenius representation (i.e., $1/T_1$ vs $1/T$) for the samples annealed at 50, 75, 125, and 250 °C. All of the experimental data were fitted using eqs 2−4, as indicated by the solid lines in Figure 6, where r_{HH}, E_a, and τ_0 were treated as variables. Figure 7 shows a plot of the activation energy (E_a) obtained from the fitting of the experimental data versus the sample annealing temperature. Clearly, E_a decreases as the annealing temperature is increased from 25 to 150 °C and reaches a minimum value of 2.47 kJ/mol at around 150 °C. E_a increases again with further increase of the annealing temperature. By comparison with the specific capacitance obtained from the $RuO_2 \cdot xH_2O$ material, shown in Figure 2, we can conclude that the activation energy is highly correlated with the specific capacitance. In fact, the activation energy corresponds to the potential barrier that hindering dynamic or diffusive motion. Therefore, the high activation energy obtained for the $RuO_2 \cdot xH_2O$ samples annealed at both low (<100 °C) and high (>200 °C) temperature indicates that the proton dynamic/diffusive motion is relatively restrained. In

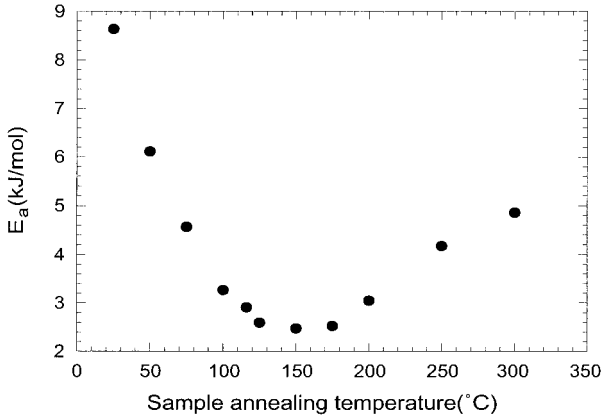

Figure 7. Activation energy (E_a) of the $RuO_2 \cdot xH_2O$ samples as a function of the sample annealing temperature.

other words, the protons have difficulty moving in the bulk of the material, thus resulting in a low specific capacitance. In contrast, for the $RuO_2 \cdot xH_2O$ samples annealed at temperatures between 100 and 200 °C, the proton activation energy is rather low, implying that the potential barrier is so low that protons can easily diffuses from one place to another, thus resulting in a high specific capacitance.

An important point to note from Figure 4 is that the value of the T_1 minimum increases significantly as the sample annealing temperature increases. As also indicated from the fitting results in Figure 6, r_{HH} was significantly shorter for the sample annealed at 25 °C (i.e., 1.306 Å) than for the sample annealed at 75 °C (i.e., 1.389 Å). However, the proton−proton distance became relatively unchanged with further increase of the annealing temperature. This implies that the local structure of $RuO_2 \cdot xH_2O$ is dependent on the sample annealing temperatures,[13] particularly in its amorphous phase. In fact, Ru is believed to be the center element in the $RuO_2 \cdot xH_2O$ materials that catalyze proton charge/discharge and proton transfer.[5] Thus, it is the local structure of $RuO_2 \cdot xH_2O$ that is associated with the proton charge and transfer ability. At the low annealing temperatures (e.g., 25 and 50 °C), the open circuit potential (E_o) measured was 0.87 V (vs SCE).[4] Thus, it is believed that the Ru^{3+} valency state dominates the local structure of $RuO_2 \cdot xH_2O$ in the presence of the overwhelming number of protons. In other words, almost every Ru forms weak hydrogen bonds with the nearby water molecules. Under these conditions, the local structure of $RuO_2 \cdot xH_2O$ becomes relatively stable. However, most of the water molecules might not directly interact with the RuO_2 lattice. Those water molecules could be nearly randomly oriented leading to a narrow ^1H line width[27] (cf. Figure 2), as if they were caged in the sieve of such a stable local structure of the material so that the protons encountered relative difficulty in moving from one place to another. This leads to a high activation energy (i.e., high potential barrier), thus resulting in low specific capacitance. However, for the sample annealed at 75 °C, the proton−proton distance was increased along with the lowering of the activation energy (cf. Figure 7). Thus, it is reasonable to assume that the local structure of $RuO_2 \cdot xH_2O$ changes in such a way that the protons of the water molecules become more involved in the local structure, with probably every water molecule now forming hydrogen bonds with the RuO_2 lattice. When the samples annealed at higher temperatures (e.g., 125 °C), the water content is further reduced so that some of the RuO_2 lattice might not have any nearby water molecules. As a result, the water molecules could exhibit relatively strong interactions with the ruthenium oxide, probably forming intermolecular hydrogen bonds with the ruthenium oxides and thus resulting in the

coexistence of the Ru^{2+}, Ru^{3+}, and Ru^{4+} valency states. In the separate open circuit potential measurements, the value of E_o obtained became 0.98 V (vs SCE),[4] which indicates that the presence of the Ru^{4+} valency state becomes relatively significant. Therefore, such a highly disordered structure allows for the valency to change easily from one state to another, as if the protons were diffusing from one site to another in the bulk of the material, while preserving the relatively strong hydrogen bonds between the water molecules and the ruthenium oxides. Consequently, the activation energy or the potential barrier becomes very low. For the samples annealed at temperatures higher than 150 °C, the water content is further reduced so that some of the local structure becomes dominated by the Ru^{4+} valency state. As a result, crystalline RuO_2 particles start to form. Such crystalline particles act as an additional barrier to proton diffusion. With an increase of the annealing temperature, the size of the particles increases so that the potential barrier becomes even higher, thus resulting in a decrease of the specific capacitance.

Conclusion

We have used solid-state ^1H NMR spectroscopy to study the proton dynamics of hydrous ruthenium oxides ($RuO_2 \cdot xH_2O$) annealed at different temperatures. To our knowledge, this is the first comprehensive study on the proton dynamics of these technologically important materials, although NMR spectroscopy has been widely used in ionic conducting materials.[28−34] Here, we experimentally obtained the activation energy (E_a) of the $RuO_2 \cdot xH_2O$ samples from the variable-temperature ^1H spin−lattice relaxation time (T_1) measurements. Our results show that the activation energy is rather low for the $RuO_2 \cdot xH_2O$ samples annealed in the temperature range of 116−175 °C but relatively high for those annealed below 100 °C and above 200 °C, which is highly consistent with the specific capacitance measurements. In fact, the activation energy is a parameter used to calibrate the potential barrier for hydrogen transfer in bulk materials. In addition, our experimental results indicate that the local structure of $RuO_2 \cdot xH_2O$ changes as the sample annealing temperature is increased, as also discussed by Mckeown et al.[13] As a result, the interaction between the structural water and the local structure of $RuO_2 \cdot xH_2O$ seems to be extremely crucial for hydrogen transfer in the bulk material.[9] Therefore, it is concluded that the activation energy obtained from the relaxation measurements not only allows us to directly measure the ability of the hydrogen transfer of the $RuO_2 \cdot xH_2O$ electrode materials but also provides insight into the structural details. This study should provide a guideline for further improvement of ruthenium oxides and also for new analogous materials based on less-expensive metallic elements.

Acknowledgment. The authors are indebted to Dr. Yan Xin of the CM/T facility at the NHMFL for the TEM measurements. This research was supported by a Program Enhancement Grant (PEG) (Project 550240537) from the Florida State University Cornerstone Programs (1999), and the work was largely performed at the National High Magnetic Field Laboratory supported by National Science Foundation Cooperative Agreement DMR-0084173 and the State of Florida.

References and Notes

(1) Conway, B. E. *Electrochemical Supercapacitors: Scientific Fundamentals and Technological Applications*; Kluwer Academic/Plenum Publishers: New York, 1999.
(2) Huggins, R. A. *Solid State Ionics* **2000**, *134*, 179.
(3) Sarangapani, S.; Tilak, B. V.; Chen, C. P. *J. Electrochem. Soc.* **1996**, *143*, 3791.
(4) Zheng, J. P.; Cygan, P. J.; Jow, T. R. *J. Electrochem. Soc.* **1995**, *142*, 2699.
(5) Zheng, J. P.; Jow, T. R. *J. Electrochem. Soc.* **1995**, *142*, L6.
(6) Zheng, J. P.; Jow, T. R.; Jia, Q. X.; Wu, X. D. *J. Electrochem. Soc.* **1996**, *143*, 1068.
(7) Zheng, J. P.; Jow, T. R. *J. Power Sources* **1996**, *62*, 155.
(8) Jow, T. R.; Zheng, J. P. *J. Electrochem. Soc.* **1998**, *145*, 49.
(9) Ma, Z.; Zheng, J. P.; Fu, R. *Chem. Phys. Lett.* **2000**, *331*, 64.
(10) Jeong, Y. U.; Manthiram, A. *Electrochem. Solid State Lett.* **2000**, *3*, 205.
(11) Rolison, D. R.; Hagans, P. L.; Swider, K. E.; Long, J. W. *Langmuir* **1999**, *15*, 774.
(12) Swider, K. E.; Merzbacher, C. I.; Hagans, P. L.; Rolison, D. R. *Chem. Mater.* **1997**, *9*, 1248.
(13) Mckeown, D. A.; Hagans, P. L.; Carette, L. P. L.; Russell, A. E.; Swider, K. E.; Rolison, D. R. *J. Phys. Chem. B* **1999**, *103*, 4825.
(14) Jow, T. R.; Zheng, J. P.; Zhang, X.; Dai, Y.; Greenbaum, S. G. *Electrochem. Soc. Proc.* **1998**, *97−24*, 442.
(15) Jackman, L. M.; Cotton, F. A. *Dynamic NMR Spectroscopy*; Academic Press: New York, 1975.
(16) Aime, S.; Gobetto, R.; Orlandi, A.; Groombridge, C. J.; Hawkes, G. E.; Mantle, M. D.; Sales, K. D. *Organometallics* **1994**, *13*, 2375.
(17) Hoelger, C. G.; Wehrle, B.; Bendict, H.; Limbach, H. H. *J. Phys. Chem.* **1994**, *98*, 843.
(18) Lipari, G.; Szabo, A. *J. Am. Chem. Soc.* **1982**, *104*, 4546.
(19) Kalk, A.; Berendsen, H. J. C. *J. Magn. Reson.* **1976**, *24*, 343.
(20) Schmidt-Rohr, K.; Spiess, H. W. *Multidimensional Solid-State NMR and Polymers*; Academic Press: New York, 1994.
(21) Gerstein, B. C.; Dybowski, C. R. *Transient Techniques in NMR of Solids: An Introduction to Theory and Practice*; Academic Press: London, 1985.
(22) Andrew, E. R.; Bradbury, A.; Geads, R. *Nature* **1958**, *182*, 1659.
(23) Xiong, J.; Lock, H.; Tao, T.; Keeler, C.; Maciel, G. E. *Solid State Nucl. Magn. Reson.* **1999**, *14*, 95.
(24) Bloembergen, N.; Purcell, E. M.; Pound, R. V. *Phys. Rev.* **1948**, *73*, 679.
(25) Kubo, R.; Tomita, K. *J. Phys. Soc. Jpn.* **1954**, *9*, 888.
(26) Solomon, I. *Phys. Rev.* **1955**, *99*, 559.
(27) Li, S. Z.; Chen, R. S.; Greenbaum, S. G. *J. Polym. Sci. B: Polym. Phys.* **1995**, *33*, 403.
(28) Figueroa, D. R.; Strange, J. H.; Wolf, D. *Phys. Rev. B* **1979**, *19*, 148.
(29) Britcher, A. R.; Strange, J. H. *Mol. Phys.* **1979**, *37*, 181.
(30) Brinkmann, D. *Prog. NMR Spectroc.* **1992**, *24*, 527.
(31) Croce, F.; Brown, S. D.; Greenbaum, S. G.; Slane, S. M.; Salomon, M. *Chem. Mater.* **1993**, *5*, 1268.
(32) Dai, Y.; Wang, Y.; Eshkenazi, V.; Peled, E.; Greenbaum, S. G. *J. Electrochem. Soc.* **1998**, *145*, 1179.
(33) Wang, Y.; Sakamoto, J.; Huang, C. K.; Surampudi, S.; Greenbaum, S. G. *Solid State Ionics* **1998**, *110*, 167.
(34) Carewska, M.; Scaccia, S.; Croce, F.; Arummugam, S.; Wang, Y.; Greenbaum, S. G. *Solid State Ionics* **1997**, *93*, 227.